Investigation on Scale Formation in Aluminium Industry by Means of a Cold-finger

Daniel Perez Clos[1], Petter Nekså[2], Sverre Gullikstad Johnsen[1,3] and Ragnhild E. Aune[1]

[1]Department of Materials Science and Engineering, Norwegian University of Science and Technology (NTNU), Trondheim, Norway
[2]SINTEF Energy Research, Trondheim, Norway
[3]SINTEF Industry, Trondheim, Norway

Communicating author: daniel.p.clos@ntnu.no

Abstract

A cylindrical fouling probe or "cold-finger" has been used to investigate fouling from aluminium production off-gas. The probe was located upstream from the off-gas cleaning system. Surface deposits have been collected for further analysis by EPMA and XRD, and compared with off-gas dust and old scale samples collected in the same experimental site. Cross-section micrographs of the deposit surfaces have been obtained to highlight the differences in surface structures formed on the upstream and downstream faces of the cold-finger. Strongly adhered hard scale formed after only two days in the upstream face of the probe. Loosely attached deposits accumulated downstream, which consisted of distinguishable particles of Al_2O_3, spherical Cryolitic bath condensates and Ni-S phases. The hard scale was rich in small bath condensates ($NaAlF_4$) that form a tight network keeping together the larger particles. The deposition of those particles is suggested to be a key in scale formation.

Keywords

Aluminium Industry, cold-finger, Fouling, Scaling

1 Introduction

The growth of hard scale in the aluminium production industry has been a problem for decades as it causes clogging in alumina transport pipes and reduces the lifetime of the off-gas filters. As a result regular shut-downs and cleaning is required, which reduces the productivity of the plant and introduces a host of other challenges [1]. It also hinders the implementation of heat recovery systems that can reduce the fraction of heat from the off-gas. Presently, this represents as much as 40% of the overall heat loss from the aluminium production [2].

It is a well-known fact that Hard Grey Scale (HGS) forms in high attrition areas, but its mechanisms and growth rates are not yet fully understood. Some previous studies have analysed old scale samples and compared them with off-gas dust to try to understand the physical and chemical differences. Dando and Lindsay [3] synthetized scale-like products by ball mixing alumina, bath fines and water, and they found that scale did not form when one of these products were lacking. As a result, they assumed that a reaction between alumina and bath fines, induced by the heat of hydration released on the newly broken alumina surfaces due to impaction, did take place.

Gaertner *et al.* [4] analysed scale and dust samples by X-Ray Diffraction (XRD) and observed that scale samples did not show the cryolite (Na_3AlF_6) peak that was present in the dust samples. They argued that moisture-induced recrystallization of cryolite -containing bath particles was important in the formation of hard scale. Although the proposed mechanisms are reasonable, no conclusive proof has so far been presented, and there are still great doubts about what are the rates in which scale grows and whether they are constant or vary with scale thickness and flow conditions.

To try to answer some of the above questions, the present study has used a cylindrical cold-finger to analyse the deposition of dust on its surface in an off-gas duct located upstream from the off-gas cleaning system at an aluminium plant. Results from 3 short-exposure experiments (2 days) have been compared with a long-exposure

This is the accepted version of an article published in The Minerals, Metals & Materials Series
DOI: 10.1007/978-3-030-05864-7_87

experiment (62 days). Moreover, off-gas dust samples have been collected and analysed together with some "old" scale, secured from the opening of the flange where the cold-finger was introduced into the duct, in order to compare the chemical composition of that scale with the cold-finger deposits.

2 Experimental

A half-meter long cylindrical cold-finger, designed and constructed at the Department of Materials Science and Engineering, Norwegian University of Science and Technology (NTNU) in Trondheim, Norway, was used in the different experiments presently reported (a detailed description of the cold-finger is presented elsewhere [5]).

During the experiments the cold-finger, consisting of an inner- and an exterior (outer) tube, was installed in an open flange in a 2.4 meters diameter duct upstream from the gas treatment center. The probe was mounted in cross-flow direction with respect to the off-gas. Initial measurements were performed to assess the off-gas velocity, which was established to be ~17.5 m/s at an average. In order to monitor the local heat transfer values from the front and rear side of the cold-finger, as well as the wall temperatures at different points, heat flux sensors and thermocouples were mounted on the surface of the cold-finger inner tube. In addition, pressurized air was circulated with a constant mass flow of ~60 l/min at a pressure of 4 bar, and the inlet temperature was equivalent to the temperature of the surrounding environment. The inlet and outlet temperatures of the coolant were also monitored allowing for the calculation of the overall heat transfer from the off-gas to the cold-finger. During the experimental trials, the overall heat flux was ~2.5 kW/m^2 and the off-gas temperature at an average ~97°C with a standard deviation of ± 5°C due to atmospheric variations. The temperature difference between the off-gas and the coolant was established to be ~85°C. The temperature difference between the wall, where the thermocouples were placed, and the off-gas was ~30°C. The actual temperature at the surface of the exterior tube where the deposition occurs was not measured, but estimated to be ~10°C. This temperature is of relevance for the calculation of the thermophoresis affecting the particle deposition.

When introducing the cold-finger for the first time into the duct through the opening of an existing flange, some "old" scale was collected and later characterized (from here on referred to as "scale flange 1"). In addition, a second "old" scale sample was collected from a screw in an adjacent flange used to introduce an instrument to iso-kinetically extract off-gas and collect dust samples (from here on referred to as "scale flange 2"). During a sampling period of two hours ~1.75 mg of dust was collected on the filter of the instrument mounted in this flange.

For XRD measurements, the samples were crushed with a mortar and loaded into the sample holder using a back-loader type. The samples were stored in a sample changer until measurement. A D8 A25 DaVinci X-ray Diffractometer with CuKα radiation LynxEye™ SuperSpeed Detector was used with a 60 minutes acquisition time and a theta range of 10-75° with a step size of 0.013°.

A JEOL JXA-8500F Electron Probe Micro analyzer (EPMA) was used in the elemental quantification by EDS and WDS and to obtain the back-scattered electron (BS-SEM) images. A 15kV acceleration voltage was used with 20nA beam current and variations of spot mode and defocus beam depending on the sample.

Energy Dispersive spectroscopy (EDS) scans were used to perform a semi-quantitative analysis of the elemental composition with a scan magnification of 1000x which allowed for a representative area to be analyzed. Wavelength Dispersive Spectroscopy (WDS) could not be used for the suspended powders since the scan area was too small to be representative. WDS was used to analyze the composition of individual particles and scale samples which were compact enough for representative averaging. For scale samples EDS and WDS were in good agreement for all elements except Sulfur which was found in lower amounts (80% lower) in WDS measurements.

The different powders and scale fragments were suspended in epoxy and polished in order to expose a flat enough surface for composition analysis using EPMA. A large piece of scale from "scale flange 1" was directly embedded into epoxy which allowed us to see in detail the stratification visible to the naked eye. SiC polishing papers where used to obtain a surface roughness of 1 μm.

An overview of the different cold-finger experiments and samples collected is displayed in Table 1.

This is the accepted version of an article published in The Minerals, Metals & Materials Series
DOI: 10.1007/978-3-030-05864-7_87

Table 1. Sample names and acquisition time (i.e. cold-finger exposure time) or site of collection for "old" scale samples.

E1	E2	E3	E4	Off-gas	Scale (flange 1)	Scale (flange 2)
2-days	2-days	62-days	2-days	2-hours	Flange walls	Flange screw

3 Results and discussion

3.1 Morphology comparison between different deposits

Based on the EPMA analyses of the collected samples it was established that four different types of particles with different morphology and composition were present. The first type was spherical and rich in Na, Al and F, but low in O. These particles are believed to be the result of droplet condensation from the cryolite bath followed by subsequent solidification due to their composition and their spherical shape. The second type of particles was non-spherical and rich in Al and O, and is believed to originate from the fine alumina (Al_2O_3) particles that are fed to the pot cells. The third kind of particles was small (< 3 μm) and rich in Ni and S, and they appear bright in colour in the BS-SEM images due to their high atomic weight. Some of them also contained large amounts of Fe. Finally, a small fraction of carbon rich micron-sized particles, believed to originate from anode dust, was also identified. These particles were difficult to spot in the BS-SEM images due to their lower atomic weight, which made them appear dark and difficult to distinguish from the epoxy-filled pores.

Representative BS-SEM images from the different samples collected during the experiments are presented in Figure 1, and the following observations were made:

When comparing the off-gas dust particles in images *A* and *B* with deposits from the rear side of the cold-finger presented in images *C* and *D* it was seen that the largest particles (> 5 μm), which were abundant in the off-gas dust, were scarce in the deposits. This is believed to be the result of the lager particles ability to escape the recirculation zone formed in the wake of the cold-finger. Given the shape of these particles, it can be deduced that they mainly consists of alumina although some bath particles can also be seen. Moreover, there was an abundance of small spherical particles in the rear deposits that cannot be seen in the off-gas sample. This is likely due to the small particles agglomerating in the surface of the larger ones when trapped in the filter upon collection.

The morphology of the scale samples in images *E* to *H* proved to differ significantly from the off-gas particles presented in images *A* and *B*, even though a granular morphology was still seen in the zoomed images (F and H). The scale samples from the 2-days experiment presented in images *E* and *F* and from the 62-days experiment presented in images *G* and *H* proved to be qualitatively very similar in size and shape with a layered growth.

The "old" scale from flange 1 in images *I* and *J* did also show layered growth, but the overall morphology was more compact resulting in that the granular structure could barely be seen in the zoomed images.

The "old" scale sample from flange 2 in images *K* and *L* proved to have a rather different morphology with flake-like agglomerates clamped together in a random way.

In Figure 2 and Figure 3 cross-sectional BS-SEM images of the deposits from one of the 2-days experiments (sample *E2*) and from the 62-days experiment (sample *E3*) are presented, respectively. In these images, the cold-finger body appears as a bright white region due to the relatively higher atomic weight of the steel tube compared to the deposits. A 100 μm thick layer of scale was found to have deposited after the 2-days experiment, whereas after the 62-days one, a maximum thickness in the front region of more than 600 μm was obtained. From visual inspection of sample *E3* upon extraction of the cold-finger from the flange, it was seen that the scale had built up to thicknesses between 2 and 3 cm. Unfortunately some of the outer layers fell-off during extraction, which revealed a cross section that consisted of layers visible to the naked eye. It should in this regard be mentioned, that the process of tube splitting, epoxy embedding and tube slicing caused the weakly adhered outer layers to even further be lost. The clear angle formed at the front side of sample *E3*, seen in Figure 2 image *C*, is believed to be the result of the merger of two crystal-like planes growing from the stagnation point where the off-gas impinges the tube. Furthermore, the layers proved to grow thinner towards the tube sides until they totally disappear somewhere around 75° from the axial flow-direction. BS-SEM images from the rear sides can also be seen for both experiments. The clean surface on the tube sides shows the cleaning effect caused by the aerodynamic shear stripping.

This is the accepted version of an article published in The Minerals, Metals & Materials Series
DOI: 10.1007/978-3-030-05864-7_87

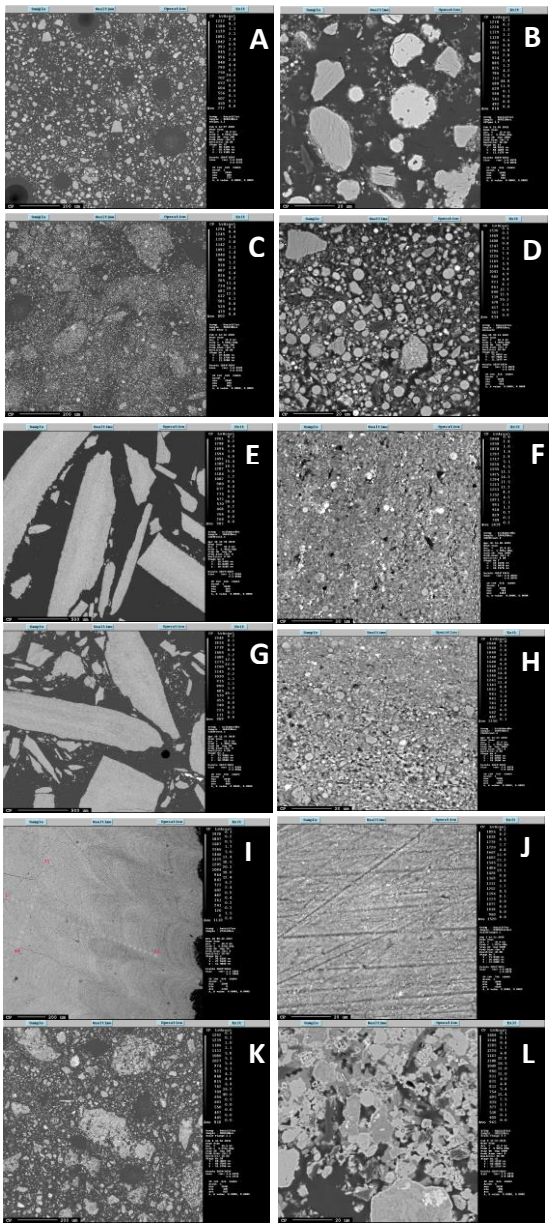

Figure 1. BS-SEM images for the different samples: off-gas dust (*A* and *B*), rear soft deposits from 2-days experiment (*C* and *D*), front scale deposits from the 2-days experiment (*E* and *F*), front scale deposits from 62-day experiment (*G* and *H*), old scale from flange 1 (*I* and *J*), and old scale from flange 2 (*K* and *L*). Left images 200 μm size bar, right images 20 μm size bar.

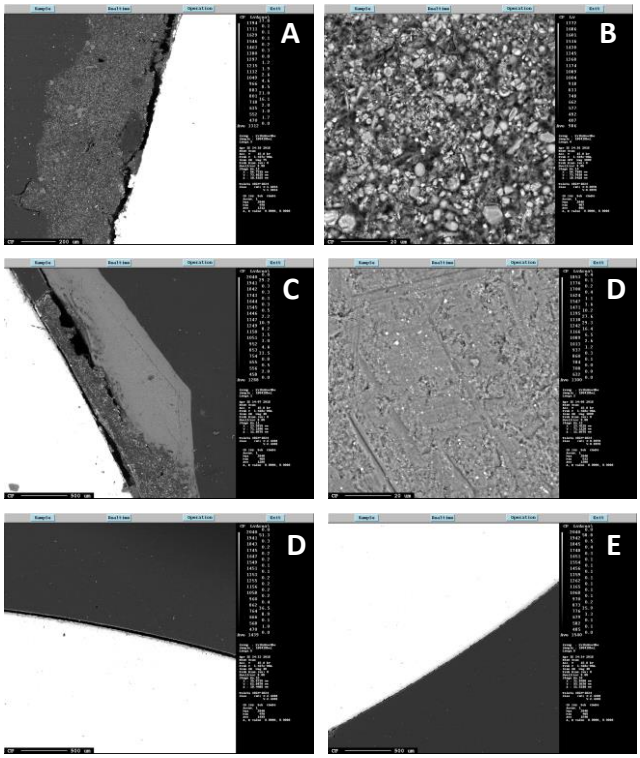

Figure 2. Cross-sectional BS-SEM images of the long-time experiments (62-days). (*A*) Rear side; (*B*) Rear side zoomed in; (*C*) Front side, (*D*) Front side zoomed in; (*E*) Upper side; (*F*) Lower side. Left images 500 μm size bar, right images 20 μm size bar.

.

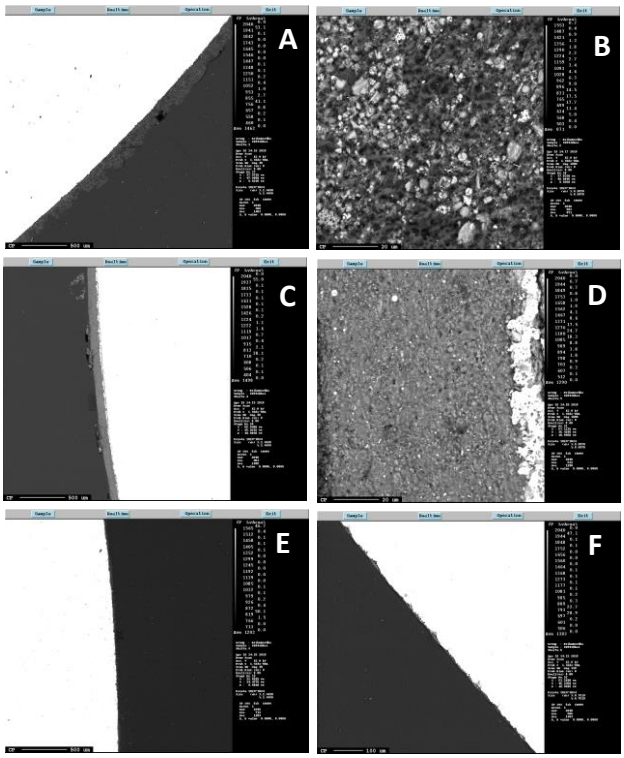

Figure 3. Cross-sectional BS-SEM images from the short-time experiments (2-days). (*A*) Rear side; (*B*) Rear side zoomed in; (*C*) Front side; (*D*) Front side zoomed in; (*E*) Upper side; (*F*) Lower side. Left images 500 μm size bar, right images 20 μm size bar.

This is the accepted version of an article published in The Minerals, Metals & Materials Series
DOI: 10.1007/978-3-030-05864-7_87

Figure 4. BS-SEM image of scale pieces from experiment *E4* (2-days) with measured thicknesses in the growth direction (500 µm size bar).

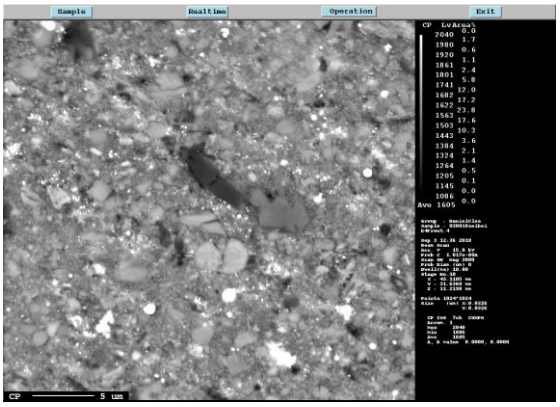

Figure 5. BS-SEM image close to the surface of scale sample *E4* (2-days) where some C particles can be seen (magnification 3000x, 5 µm size bar).

In Figure 4 a BS-SEM image of the front deposits from one of the 2-days experiments (sample *E4*) is presented. As can be seen from the figure scale pieces as thick as 300 µm in the growth direction were obtained. This suggests an initial growth rate of 150 µm/day, which would scale up to 9.3 mm after 62 days at a linear rate. Considering that the actual observed layers in the 62-days experimental data were at least 2 to 3 times this value, this suggests an increasing scaling rate over time that provably originates from the increased stickiness of the scale-covered surfaces.

Samples of the interface between the deposit and the metal proved to be quite difficult to secure due to the coarse treatment needed to extract the cold-finger from the duct. In the zoomed BS-SEM image *D* of Figure 3 the rough metal surface of this area can be seen, as well as the metal interface attached to the scale. From the figure, it can be observed that the metal surface seems to be detached from the steel core of the tube at most of the interface. It should in this regard be mentioned that plant operators have reported that oxide layers do exist between the scale deposits and the wall, which could explain why this layer would detach from the metal core while still being attached to the scale layers. From Figure 3 BS-SEM image *D* it can also be seen that most particles close to the surface are smaller than the cavities formed in the metal surface. Larger particles are also seen scattered away from the interface, but there is a clear abundance of sub-micron particles forming a tight web that seems to keep the other phases bounded together. A web of finer particles can also be seen in the zoomed BS-SEM image of a scale piece surface in Figure 5, together with a large C particle in the center of the image and a few smaller ones around.

3.2 Element composition and crystal phases

3.2.1 EPMA

The average composition of the main elements present in the different types of particles established to exist in the different kinds of samples has been analysed by both EDS and WDS, and the results are presented in Table 2. It should be mentioned that C was not included in the analysis both due to the difficulties of quantifying this low atomic weight element, as well as the fact that the C-rich epoxy matrix would add up to the quantitation (especially in the case of the powder suspended samples). The qualitative EDS results however, did confirm the presence of C in the C particles that did not show the presence of any other main elements. As can be seen from Table 2, the bath particles consist mainly of Al, Na and F with low amounts of O. The alumina (Al_2O_3) particles are of course rich in Al and O, but notorious amounts of F were also found that most likely originates from the HF condensation given the low amount of Na. Finally, most of the bright particles analysed showed a composition close to the Ni-S (nickel-sulfur) particles, whereas a few also contained a large amount of Fe. Thus, in Table 2 these particles have been classified into different categories.

This is the accepted version of an article published in The Minerals, Metals & Materials Series
DOI: 10.1007/978-3-030-05864-7_87

Table 2. Averaged elemental analyses in mass percentage (mass-%) of the different types of particles present in the scale from different samples and experiments (based on both EDS and WDS results).

Element	Bath spherical particles (mass-%)	Alumina particles (mass-%)	Nickel-sulfur particles (mass-%)	Nickel-sulfur-iron particles (mass-%)	Carbon particles (mass-%)
Al	29.2	46.6	1.3	1.2	0.3
Na	24.5	1.8	0.7	0.5	0.1
F	28.3	8.9	0.6	0.4	0.3
O	5.2	32.4	1.0	1.2	0.5
S	0.8	0.8	39.4	32.0	1.4
Ni	0.3	0.1	54.0	36.5	0.0
Fe	0.3	0.1	1.1	24.8	0.0
Ca	3.3	0.1	0.0	0.0	0.0

In Table 3 the compositional analyses of the different sample types secured from the experiments performed, have been averaged to see if any differences exists between the types of deposits and the free particles. As can be seen from the table, some differences do exits especially when comparing the scaling sample results with the off-gas composition (there is larger amounts of Al and O in the off-gas). This is in good agreement with the morphological observations made of the larger fraction of particles, which could be seen in the off-gas but were missing in the rear deposits. The explanation presented earlier in regards to the larger size alumina particles being trapped by the tube wake on the rear side of the cold-finger cannot be applied to the front side case where the larger particles are likely to impact the surface due to their size. However, it can be reasoned that the larger particles might impact the surface with too large velocities for them to adhere to the wall and thus, bounce off instead. The other main difference is the larger amount of S in the deposits compared with the off-gas, which also have been observed in previous scale studies [4]. This has in the research community generated the idea that S might be a key element in scale formation in aluminium production off-gas systems. In this regards it should be mentioned that the analysis of the composition of individual particles presented in Table 2 shows that the amount of S contained in those particles is < 1%. Since the mass-percentage of S in the off-gas is ~4%, that means that ~75% of the S must come from the bright particles or other S containing particles. The role of bright particles in scale formation does not seem important since they do not accumulate on any specific location.

The scale from flange 1 has a very similar composition to the cold-finger deposits except for a higher amount of S. The scale from flange 2, however, has higher amounts of F and O, which is in accordance with the presence of specific crystal phase not found in any of the other samples as will be shown in the next section.

Table 3. Averaged element analyses in mass percentage (mass-%) of the different types of samples (based on semi-quantitative EDS results in areas with magnification 1000x).

Element	Samples front (mass-%)	Samples rear (mass-%)	Off-gas (mass-%)	Scale flange 1 (mass-%)	Scale flange 2 (mass-%)
Al	27.1	26.1	34.3	24.4	23.5
Na	12.8	13.3	8.7	12.9	11.5
F	30.3	32.3	25.7	31.1	42.1
O	15.9	15.7	25.3	15.8	18.9
S	7.4	6.7	3.8	12.8	1.5
Ni	2.2	2.0	0.8	1.0	0.4
Fe	2.6	2.1	0.5	1.2	0.4
Ca	0.5	0.8	0.6	0.0	1.4

This is the accepted version of an article published in The Minerals, Metals & Materials Series
DOI: 10.1007/978-3-030-05864-7_87

3.2.2 XRD

In Figure 6 representative XRD scans for some of the collected samples are presented. It should be noted that the scale sample from the first 2-days experiment, i.e. sample *E1*, was so thin that it went unnoticed and no sample was therefore collected. Some scale was, however, collected from the second 2-days experiment, i.e. sample *E4*, but the amount was limited and only EPMA analysis could therefore be performed.

Based on the XRD scans a peak intensity-based semi-quantitative analysis was performed and the results are presented in Table 4. It should in this regard be mentioned that to be able to perform a reproducible and exact semi-quantitative analysis it is a requirement that all the phases present can be identified and that not too much overlapping and peak broadening exists. This is, however, not the case for the present samples, which all show very complex scan patterns. The reported results in Table 4 should therefore be taken with certain care.

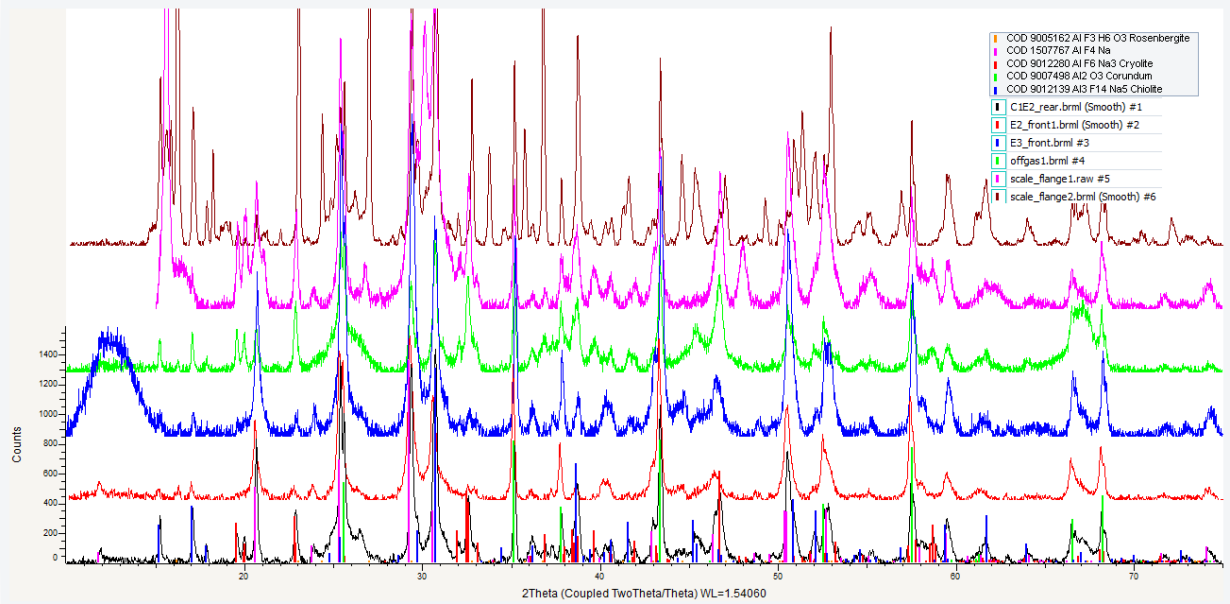

Figure 6. XRD scans for the different samples collected. *E2* front (red) and rear (black), *E3* front (blue), off-gas (green), and scale flange 1(pink) and 2 (brown).

Table 4. Semi-quantification of the different phases found in the XRD spectra of the different samples in mass percentage (mass-%).

Phase	E1 rear (mass%)	E2 rear (mass%)	E2 front (mass%)	E3 front (mass%)	E3 rear (mass%)	E4 rear (mass-%)	Off-gas (mass%)	Scale flange 1 (mass%)	Scale flange 2 (mass%)
Na_3AlF_6 (Cryolite)	24.1	20.7	8.8	7.4	22.4	19.0	29.9	26.6	2.4
$Na_5Al_3F_{14}$ (Chiolite)	18.6	18.8	13.6	4.1	15.6	15.7	13.8	8.0	24.0
Al_2O_3 (alumina)	16.8	19.5	31.4	26.1	14.9	12.8	27.4	12.9	13.9
$NaAlF_4$	19.7	17.4	22.4	26.0	13.7	14.7	8.2	16.6	2.8
Carbon phases	13.0	16.3	14.7	30.7	28.4	31.8	13.1	30.0	18.5
H_3NaO_5S (Matteuccite)	4.6	4.1	2.9	3.1	3.2	4.2	4.0	1.1	2.2
AlF_3	1.8	2.0	3.1	1.1	0.6	0.7	1.8	1.6	0.4
$AlF_3H_6O_3$ (Rosenbergite)	0.4	0.2	1.7	0.6	0.6	0.4	1.1	2.6	35.0
Ni_3S_2 + $FeNiS_2$	1.2	0.7	1.5	0.9	0.6	0.9	0.9	0.6	0.8

This is the accepted version of an article published in The Minerals, Metals & Materials Series
DOI: 10.1007/978-3-030-05864-7_87

A characteristic feature of scale XRD scans is the weakening of the cryolite (Na_3AlF_6) peaks that otherwise are very intense in off-gas dust samples [4]. This is also the case in the present results as can be seen from Figure 6, *i.e.* both samples *E1* rear and off-gas show a large cryolite peak that is almost faded in samples *E2* front and *E3* front. On a more quantitative basis, the off-gas has the largest cryolite peak (~30%) whereas the cold-finger scale samples and the scale from flange 2 have a much lower concentrations (~8%). The strong presence of cryolite in the "old" scale collected from the flange walls, *i.e.* scale flange 1, was not expected considering the morphological and compositional resemblances with the cold-finger scale samples. A possible explanation for this observation is that some off-gas dust that had deposited around the flange scale layers could have been mixed up with the scale samples during collection. The "old" scale collected from the flange screw, *i.e.* scale flange 2, revealed a completely different morphological and compositional structure, as well as the presence of a main crystal phase only present in small amounts in the off-gas and the other scale samples. A clear and almost perfect fit to multiple peaks of different intensities showed the presence of Rosenbergite, a hydrolysed version of AlF_3. As the screw was regularly removed from the flange off-gas dust sampling, it seems reasonable to assume that the dust accumulated in the screw could have been exposed to air humidity and rain, which could have affected the nature of the scale in such a way.

The carbon (C) phases present in the samples proved to be difficult to identify and to quantify since they were represented by a large number of overlapping XRD-peaks. This suggests the presence of rather similar C structures. It should, however, be mentioned that C phase values are probably under-estimated since it was not possible to find phases that covered some of the regions without having non-existing satellite peaks.

As can be seen from table 4, S is mainly present in some of the carbon phases and then in the form of the phase Matteucite. The XRD peaks assigned to the Ni-S-Fe phases (bright particles) only amount to 0.4 mass % of S in the sample which is only ~10% of the overall S content measured by EPMA.

Another interesting aspect from Table 4 is the low amount of $NaAlF_4$ present in the off-gas compared to most of the other samples (except for "scale flange 2"). This is can be explained by the previous observations made in regards to the larger particles not depositing on the front nor on the rear side of the screw. Most of them consist of alumina although some large bath particles are present as well. Given their larger size and not so perfectly spherical shape, they might consist of cryolite liquid bath or solid crust particles entrained by the air draft. Therefore, the relative large amounts of cryolite and alumina in the off-gas might be reduced in the deposits in favour of $NaAlF_4$. It has previously been shown by Gaertner *et al.* [6] that $NaAlF_4$ is mainly present in the finer fractions of the off-gas particulates, *i.e.* the particles that can be seen all over the front and rear deposits of the cold-finger. As previously mentioned, the small size of these particles makes them stickier due to the large-surface to volume ratio. Their high concentration in the rear side deposits can be explained by entrapment in the recirculation zone formed in the wake of the cold-finger. Their presence in the front side suggest that their inertia in this area is large enough to break from the streamlines circumvallating the tube despite their small size. Another explanation may be that these particles reach the front wall while adsorbed to the surface of larger particles.

The previously proposed scaling mechanism by Gaertner *et al.* [4], suggesting that cryolite particles recrystallize into chiolite in the presence of AlF_3 and moisture, might be put to question by the presence of cryolite in "scale flange 1" (if that is indeed the case). Moreover, the fact that the cryolite levels are virtually the same in the fresh 2-days scale (E2) and the older 62-days scale (E3) do not support that theory either, unless only the 65% of deposited cryolite is available for reaction and does it so "instantaneously" as it deposits. Since such a reaction requires the formation of AlF_3 from alumina, for further reaction with cryolite, such fast reactions rates are difficult to believe. Moreover, the amount of suggested final product chiolite does not increase in the analysed scale samples.

Another possible mechanism for scale formation of a more mechanical nature is proposed if we consider that the lack of cryolite is due to e.g. the size or shape of cryolite containing particles making them unsuitable for deposition in the front side. It could therefore be thought as the smaller size fraction of bath particles consisting mainly of $NaAlF_4$, being the "glue" that allows larger particles to stick together. This would be backed up from observation of zoomed scale surfaces (Figure 5) and the larger amount of $NaAlF_4$ in the deposits. Moreover, as was shown by [6], the fine-particle fraction forms "needle-shaped fibrous frameworks with knobbly or grape-like droplets with smaller particulates attached". Such fibrous particle networks might be adsorbed on the surface by larger, inertial particles, making them sticky and enhancing their adhesion to the deposit surface. Further, dynamic pressure from the off-gas flow and particle impaction might lead to the final compact hard scale. Rear deposits would thus keep their soft and dusty nature due to the lack of dynamic pressure in this area.

This is the accepted version of an article published in The Minerals, Metals & Materials Series
DOI: 10.1007/978-3-030-05864-7_87

A fluid dynamics-based description of particle transport in cylinder cross-flow will be developed to understand how the ability to get close to the wall and deposit, for particles of different sizes, depends on the circumferential position of the probe.

Chemical reactions should not be ruled out as playing an important role in scale formation until the reason for the lack of cryolite in scale is completely understood. However, reactions involving multiple solid phases need to be considered with care. It has been shown that the different types of particles have small amounts of other phases probably due to surface adsorption of smaller particles. This would allow surface exposure between different phases with subsequent chemical reactions. However, the bulk of material for the different phases is still contained within the particles, which do not seem to merge into each other when looking at a close image from a scale grain (Figure 5). Even the smallest particles that can be identified in the image seem to keep their particle boundaries intact rendering further reactions with other phases challenging.

3.2.3 Comparison between EDS and XRD results

To be able to compare the presently obtained analytical results, the quantified crystal phases from the XRD scans have been translated into elemental compositions and added together with the EDS values for some of the samples, as can be seen in Table 5.

Overall a "good agreement" between the techniques is obtained with some minor deviations, which is expected considering that none of the techniques offer optimal conditions for a more exact quantification. The use of a better epoxy and finer polishing grains could improve the EPMA analysis whereas a Rietveld-like phase quantification could also help in better quantifying the relative amounts of the different crystal phases.

Table 5. Compositional analysis in mass percentage (mass-%) based on measured Energy-Dispersive X-ray Spectroscopy (EDS) results and calculated elemental analyses from the XRD crystal phases identified in the different samples.

Element	E2 rear (mass-%)		E2 front (mass-%)		Off-gas (mass-%)		Scale flange 1 (mass-%)		Scale flange 2 (mass-%)	
	EDS	XRD	EDS	XRD	EDS	XRD	EDS	XRD	EDS	XRD
Al	28.1	20.7	28.0	26.2	26.9	23.3	24.4	16.2	23.5	19.4
Na	12.3	15.3	12.2	10.8	12.5	15.4	12.9	13.9	11.5	7.6
F	31.7	34.0	28.3	28.9	31.3	30.8	31.1	31.2	42.1	31.5
O	17.1	16.7	18.7	21.3	15.3	19.7	15.8	15.9	18.9	25.6
S	5.5	2.2	8.3	1.7	6.7	1.7	12.8	3.2	1.5	1.4
Ni	1.6	0.4	1.6	0.9	2.4	0.5	1.0	0.4	0.4	0.5
Fe	1.9	0.1	1.8	0.2	2.8	0.1	1.2	0.1	0.4	0.1
Ca	1.0	0.0	0.1	0.0	0.8	0.0	0.0	0.0	1.4	0.0
C	NA	8.1	NA	8.0	NA	6.9	NA	15.5	NA	10.4
H	NA	0.9	NA	1.0	NA	0.8	NA	2.1	NA	2.7
N	NA	1.3	NA	1.1	NA	0.9	NA	1.5	NA	0.7

4 Conclusions

In the present study a cylindrical cold-finger has been used to analyse the deposition of dust/scale on its surface when exposed to off-gas in cross-flow direction in a duct located upstream from the off-gas cleaning system at an aluminium plant. The following conclusions have been drawn:

- The off-gas particles consist of four different kind of particles with distinguished composition, *i.e.* large unstructured Al_2O_3 particles, smaller spherical bath condensates consisting of Al-Na-F phases, smaller particles consisting of primarily S and Ni, as well as scarce C particles.
- Soft and dusty deposits accumulate on the downstream side of the cold-finger. Their characteristics are quite similar to the free particles in the off-gas, and it is possible to identify different types of particles. However, a range of larger particles mainly consisting of Al_2O_3 from the off-gas (10-20 µm) are not present in the rear deposits, which is in agreement with the averaged chemical analysis that shows larger levels of Al and O for the off-gas compared to both the rear and front deposits.

This is the accepted version of an article published in The Minerals, Metals & Materials Series
DOI: 10.1007/978-3-030-05864-7_87

- Scale is formed already after 2-days with a thickness up to ~300 μm. The 62-days sample was 2 to 3 cm thick indicating an increasing scaling rate over time. Scale morphology is rather compact where the different types of particles become difficult to appreciate in some regions. Layered growth is seen, which suggests an ordered packing of particles of similar size in specific and ordered growth directions.
- The levels of sulfur (S) in the front scale samples and rear deposits are very similar, but significantly larger than the ones in the off-gas particles. Sulfur is mainly present in the carbon phases, as well as in the form of Matteucite phase. Sulfur from Fe-Ni-S particles have also been identified in low amounts. Such particles do not seem to agglomerate in any particular region in scale surfaces and therefore are not believed to play an important role on scale formation.
- The amounts of cryolite (Na_3AlF_6) found in the deposits after both 2- and 62-days exposer have the same low levels compared to the larger amounts found in the off-gas dust. The fact that the cryolite levels do not decrease for the long-exposure case indicates that no specific reaction is taking place over time. It is therefore proposed that cryolite particles might not deposit on the front side of the cold-finger due to their size and shape characteristics.
- Scale samples contains large amounts of very small bath particles ($NaAlF_4$) which, given their size and shape, seem to be the key ingredient in holding together the larger grains. The prolonged dynamic pressure from the off-gas flow and the particles impaction is suggested to yield the resulting compact hard scale.

5 Future work

Future research using computational fluid dynamics will be conducted to understand the ability of different sized particles to reach the different zones of a cylinder in a cross-flow. The results from this study will allow assessing the feasibility of the mechanism proposed in the present work in regards to scale formation. Experimental trials are also planned in order to study the effect of other parameters that may influence scale formation, *e.g.* the temperature of the cold surface or cold-finger tubes material and surface roughness.

6 Acknowledgment

The present work has been funded by the SFI Metal Production, (Centre for Research-based Innovation, 237738), and the authors gratefully acknowledge the financial support from the Research Council of Norway and the partners of the SFI Metal Production. The contributions from Eirik Nordbø for the help during the setup, building and experimental trials are also highly acknowledged.

7 References

1. Bott, T.R., *Fouling of Heat Exchangers*, in *Fouling of Heat Exchangers*, T.R. Bott, Editor. 1995, Elsevier Science B.V.: Amsterdam.
2. Grjotheim, K. and H. Kvande, *Introduction to aluminium electrolysis : Understanding the Hall-Hérloult process*. 1993, Düsseldorf: Aluminium-Verlag.
3. Dando, N.R. and S.J. Lindsay, *Hard Gray Scale*, in *Essential Readings in Light Metals: Volume 2 Aluminum Reduction Technology*, G. Bearne, M. Dupuis, and G. Tarcy, Editors. 2016, Springer International Publishing: Cham. p. 602-607.
4. Gaertner, H., A.P. Ratvik, and T.A. Aarhaug, *Raw Gas Particles and Depositions in Fume Treatment Facilities in Aluminium Smelting*, in *Light Metals 2014*, J. Grandfield, Editor. 2014, Springer International Publishing: Cham. p. 547-552.
5. Clos, D.P., Gaertner, H., Nekså, P., Johnsen, S.G., Aune, R.E., *Design of a cooled fouling probe to investigate scaling mechanisms from the aluminiuim production off-gas*, in *Heat Exchanger Fouling and Cleaning*. 2017: Madrid.
6. Gaertner, H., A.P. Ratvik, and T.A. Aarhaug, *Impurity Elements in Raw Gas Ultra-Fines from Aluminium Electrolysis Cells*, in *Light Metals 2012*, C.E. Suarez, Editor. 2012, Springer International Publishing: Cham. p. 839-844.

This is the accepted version of an article published in The Minerals, Metals & Materials Series
DOI: 10.1007/978-3-030-05864-7_87